JOURNAL OF PROPULSION AND POWER
Vol. 21, No. 3, May–June 2005

Aerodynamic Experiment on an Ejector-Jet

Shigeki Aoki,* Jongsun Lee,† and Goro Masuya‡
Tohoku University, Miyagi 980-8579, Japan
and
Takeshi Kanda§ and Kenji Kudo¶
Japan Aerospace Exploration Agency, Miyagi 981-1525, Japan

Characteristics of an ejector-jet were investigated experimentally. Evaluation of a new, one-dimensional model of suction performance under the aerodynamic choking condition and observation of mixing conditions through the pseudo-shock were primary subjects of study. Supersonic primary rocket exhaust was simulated by air, and secondary airflow was simulated by nitrogen. Parameters were the ratio of the total pressure of the secondary flow to that of the primary flow, the ratio of the entrance area of the secondary flow to that of the primary flow, and the Mach number of the primary flow. A throttling valve downstream of the mixing region simulated subsonic combustion and subsequent choking, and the throttling created a pseudo-shock ahead of the valve. The suction performance increased with increased total pressure of the secondary flow, the increase of the Mach number of the primary flow, or the increase of the area of the secondary flow. The calculated results on the suction performance agreed well with these measured values. When the gases became subsonic due to throttling, the primary and secondary fluids mixed well through the pseudo-shock and became almost uniform ahead of the downstream choking position. The mixing progressed quickly in the pseudo-shock.

Nomenclature

A = cross section
H = height
M = Mach number
$\dot{m}$ = mass flow rate
P = pressure
P_t = total pressure
r = ratio of the mass flow rate of the secondary flow to that of the primary flow
T = temperature
T_t = total temperature
u = velocity
x = streamwise coordinate from the entrance of the test section
y = vertical coordinate from the primary-flow sidewall
z = spanwise coordinate from the center plane of the test section
γ = ratio of specific heats
ρ = density
ω = mass fraction of the secondary flow

Subscripts

ch = choking of the secondary flow
th = downstream throat
th1 = throat of the primary-flow nozzle
w = wall
1 = primary fluid
2 = secondary fluid
3 = mixed fluid

Presented as Paper 2003-0188 at the 41st Aerospace Sciences Meeting and Exhibit, Reno, NV, 6–9 January 2003; received 27 November 2003; revision received 6 December 2004; accepted for publication 8 December 2004.

*Graduate Student, Department of Aeronautics and Space Engineering, 1 Aramaki, Aoba, Sendai; currently, Research Engineer, Gas Turbine Division, Kawasaki Heavy Industry Co., Ltd., 1-1, Kawasaki, Akashi, Hyogo 673-8666, Japan.

†Graduate Student, Department of Aeronautics and Space Engineering, 1 Aramaki, Aoba, Sendai; currently, Research Engineer, Central Research Institute, Yanmar Co., Ltd., 1600 Umegahara, Maibara, Shiga 521-0013, Japan.

‡Professor, Department of Aeronautics and Space Engineering, 1 Aramaki, Aoba, Sendai; masuya@cc.mech.tohoku.ac.jp. Senior Member AIAA.

§Leader, Engine System Team, Combined Propulsion Research Unit, Space Propulsion Research Center; 1 Koganesawa, Kimigaya, Kakuda, kanda.takeshi@jaxa.jp. Senior Member AIAA.

¶Senior Researcher, Engine System Team, Combined Propulsion Research Unit, Space Propulsion Research Center, 1 Koganesawa, Kimigaya, Kakuda; kudo.kenji@jaxa.jp.

Introduction

SEVERAL kinds of airbreathing engines, for example, combined-cycle engines, for the aerospace plane have been studied.[1,2] One type of combined-cycle engine is composed of an ejector-jet mode, a ramjet mode, a scramjet mode, and a rocket mode.[3–8] Figure 1 shows a schematic of the ejector-jet mode. The ejector-jet mode is used from takeoff to about Mach 3. In this mode, the ejector effect of the primary rocket induces atmospheric air. Not only the rocket engine itself, but also the diffuser section produces thrust due to the increased pressure of the mixture. Studies of the ejector-jet engine have been conducted,[9–15] and studies of the ejector itself have also been carried out.[16–24] In one kind of ejector-jet engine, subsonic combustion is attained by fuel injection at the end of the diffuser section. According to a previous study of the airbreathing rocket,[10] mixing and combustion efficiency were significantly better than those in the supersonic combustion mode. In the engine with the subsonic combustion mode, the combustion gas is choked at the exit of the combustor section.

The secondary flow is entrained by the primary flow. Under some conditions, the secondary fluid flows into the ejector at subsonic speed and chokes aerodynamically due to interaction with the primary fluid. This condition is designated the aerodynamic choking mode.[16] Supersonic speed of the fluids is necessary so that the downstream high pressure due to combustion and choking does not affect the suctioning of air. For this aerodynamic choking condition, there are one-dimensional[16,17,21] and two-dimensional models using the method of characteristics.[19] The one-dimensional model, in which the isentropic process is employed throughout the interaction between the primary and the secondary flows, was used in examination of the features of the ejector or optimization of the operating conditions.[23] However, as pointed out by Fabri and Siestrunck[16] and Fabri and Paulon,[17] the actual interaction process is not isentropic. Under the coincident pressure condition, the total impulse function

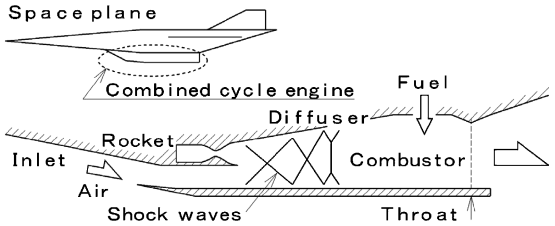

Fig. 1 Schematic diagram of space plane and ejector-jet mode of combined-cycle engine.

calculated with the model is not conserved in a duct with a constant area. Under the conserved impulse function condition, two pressures are calculated with the model for each of the primary and the secondary flows. Use of the model may yield misleading information on thrust performance or suction performance of the engine. Thus, a new model on aerodynamic choking has been proposed, in which coincident pressure is attained by conservation of the impulse function.[8] In the present study, this model is evaluated by comparing the calculated results of the model with the experimental ones for the suction performance.

In the subsonic combustion mode, the primary and the secondary flows become subsonic as they pass through the pseudo-shock.[25] In the pseudo-shock, mixing enhancement is anticipated due to an increase of turbulence.[26,27] In the ejector-jet engine or airbreathing rocket engine with subsonic secondary combustion, mixing conditions have been investigated experimentally, although relatively few experiments have been conducted.[10,14] Most studies of the pseudo-shock have used a single fluid. Two fluids are used in the pseudo-shock study of the ejector, but mixing of the fluids has not been investigated. In the study of shock-enhanced mixing,[28] fluid is a fuel jet, its volume flow rate is much smaller than the primary flow, and there is no pseudo-shock, except in the study of fuel injection into the pseudo-shock.[27] In the present study, the mixing process of the fluids as they pass through the pseudo-shock was also investigated, when the fluids have a similar volume flow rate at the beginning of the interaction.

The authors conducted aerodynamic tests of the ejector-jet. The effect of subsonic combustion and subsequent choking was simulated by a valve at the exit of the test section, which created a pseudo-shock ahead of the valve. The experimental results were compared with those calculated by the models. The mixing condition was examined with gas sampling and pitot pressure measurement. The parameters in the experiments were the ratio of total pressure of the secondary flow to that of the primary flow, the ratio of the entrance area of the secondary flow to that of the primary flow, and the Mach number of the primary flow.

Experimental Apparatus

Test Facility

Figure 2 shows a schematic of the ejector-jet test facility. It consists of a primary supersonic nozzle, a secondary flow supply system, a test section, and a downstream throat section. The primary-flow, which is rocket exhaust in an actual engine, was simulated by air. Nitrogen was used as the secondary flow, which is air in the actual engine. A pressure- regulating valve controlled the mass flow rate of the secondary flow. The ratio of the total pressure of the secondary flow to that of the primary flow was controlled to be 0.01–0.2. Total temperature of the primary flow and the secondary flow was around 290 K.

The entrance of the primary flow duct was 25 mm in height and 50 mm in width. Two primary nozzles were used to facilitate changing of the entrance Mach number of the primary flow to Mach 2.4 or 3.4. The 99% velocity boundary-layer thickness of the Mach 2.4 flow and that of the Mach 3.4 flow were 4.2 and 5.0 mm, respectively. The unit Reynolds numbers were 5.7×10^7 m^{-1} and 9.8×10^7 m^{-1}, respectively. The entrance of the secondary flow duct was 46 mm in width. The height of the secondary flow duct, which was a parameter, was 15.5, 22, or 30 mm. The unit Reynolds number of the secondary flow was 1.0×10^4–2.0×10^6 m^{-1}. The test section

Table 1 Geometrical configuration of the test section[a]

H_2, mm	A_2/A_1 at entrance	H_{th}/H_1		H_{th}/H_2	
		No throttling	Throttling	No throttling	Throttling
15.5	0.57	1.72	1.34	2.77	2.16
22	0.81	2.00	1.56	2.27	1.77
30	1.10	2.28	1.78	1.9	1.48

[a]Under throttling condition at downstream throat, $H_{th}/H_3 = 0.78$. Under no throttling condition, $H_{th} = H_3$.

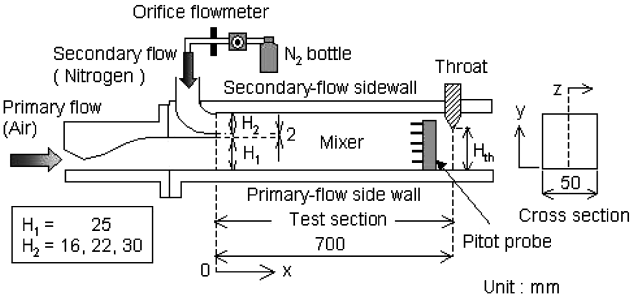

Fig. 2 Schematic diagram of experimental facility.

was a straight rectangular duct. The 99% velocity boundary layer of the secondary flow was 8 mm. The displacement thickness was estimated to be about 1.5 mm in the subsonic to sonic flow conditions. When the 15.5-mm duct was used, the viscous effect was more obvious. In the present study, the mixing condition through the pseudo-shock under the choking condition was compared with that in the shear layer with no choking. Therefore, the thickness of the boundary layer does not greatly affect the discussion here. In the calculation models to be described, the Mach number based on the measured mass flow rate was used.

The downstream throat was positioned at 700 mm from the entrance of the test section. The ratio of the cross section at the throat to that in the test section, H_{th}/H_3, was 0.78. Based on the ratio of the cross sections, calculation showed the Mach number of the mixture in the test section to be 0.53. The throttling at the downstream throat in the present cold-flow experiment corresponds to changes of the equivalence ratio, the enthalpy level of the inflow air, and the contraction ratio of the second throat in an actual engine. In the present study, throttling was not adopted as a parameter and the contraction at the second throat was fixed. Table 1 lists geometrical configurations of the present experiment.

Measurements

Schlieren Photographs

Spark schlieren photographs were taken for the area from $x = 0$ to 140 mm to observe the flowfield around the entrance of the test section. The pulse time of the stroboscope lamp was 60 ns.

Wall Pressure

The sidewall pressure was measured along the centerlines of the primary flow and the secondary flow at every 20-mm interval. A mechanical scanner (Scanni Valve®) was used with a scanning rate of 0.2 s per port and a sampling frequency of 50 Hz. The measurement uncertainty was ±1.4 kPa.

Mass Flux Measurements

The primary mass flux was estimated to an accuracy of ±0.3% using measured stagnation properties and a choked nozzle formula. The secondary mass flux was measured to an accuracy of ±0.5% using an orifice flowmeter inserted into the nitrogen supply line. Mach number and total pressure of the secondary flow were estimated using the mass flux and the wall pressure measured at $x = -10$ mm.

Pitot Pressure and Gas Composition

Pitot pressure measurement and gas sampling were conducted on the centerline at $x/H_1 = 6.0$, 14.0, 22.0, and 25.2. The error of the pitot pressure was the same as that of the wall pressure due to

the use of the same pressure sensor. Gas was sampled by the pitot probe and analyzed by gas chromatography (Micro-GC CP-2002®). Based on pitot pressure and gas compositions, the total pressure, Mach number, mass flux, and mixing condition were investigated. The wall pressure was used instead of the static pressure.

Models for Calculation of Suction Performance

Downstream Choking Model: Model A

This model is a general one-dimensional model for two-fluid mixing flow.[22] In this model, choking at the downstream throat affects the entrance condition of the secondary flow. The secondary fluid flows into the test section at subsonic speed. Total pressure, total temperature, and the Mach number of the primary flow are specified, as is total pressure and total temperature of the secondary flow. The mass flow rate of the secondary flow is calculated with these boundary conditions under assumptions of complete mixing in the test section, isentropic acceleration in the convergent section, and choking at the downstream throat. Mass, momentum, and energy are conserved. Friction drag and heat transfer to the wall are ignored. The base pressure on the wall between the primary flow and the secondary flow ducts is zero for simplification.

Aerodynamic-Choking Model 1: Model B

Figure 3 shows a schematic of a simplified, aerodynamic-choking model.[8] In this model, the secondary flow is subsonic at the entrance and chokes in the test section. The choking position is indicated by e in Fig. 3. In this mode, the condition downstream of the aerodynamic choking position does not affect the condition at the entrance of the test section. In some previous one-dimensional calculation models, the isentropic process was adopted for the interaction between the primary flow and the secondary flow.[16,17,21] Actually, however, the interaction is not an isentropic process, and application of the isentropic assumption produces contradictions, for example, two different static pressures of the two flows at the end of the interaction. A new one-dimensional calculation model proposed by the Kanda and Kudo[8] uses the isentropic condition only at the beginning of the interaction. The whole process is not isentropic and a single static pressure is attained, with mass, impulse function, and energy being conserved. Boundary conditions of the primary flow are specified at the entrance. Total pressure and total temperature of the secondary flow are also specified at the entrance. The primary flow and the secondary flow do not mix, but exchange momentums. Friction drag and heat transfer to the wall are ignored for simplification.

The dividing streamline is straight for simplification in this model. First, pressure of the subsonic secondary flow at the entrance of the test section is assumed and the flow rate of the secondary fluid is calculated. The primary flow expands to the assumed pressure two dimensionally. The initial condition of the expansion process is calculated with the Prandtl–Meyer function. The dividing streamline between the primary and secondary flows is extended to the choking point of the secondary flow. The dividing streamline and the exchanged momentum are calculated using this initial condition of the interaction under the presumed pressure. After choking and the interaction, the primary fluid and the secondary fluid flow in parallel one dimensionally at the same pressure. The assumed pressure of the secondary flow is changed to conserve mass, impulse function, and energy. The total interaction process, except the initial Prandtl–Meyer expansion, is not isentropic, and the pressure at the choking point of the secondary flow is the same as that of the primary flow. As

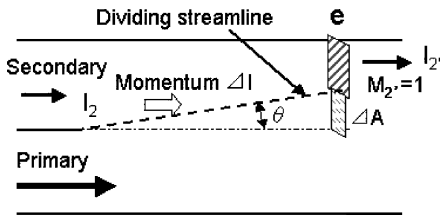

Fig. 3 Schematic diagram of model b for simulation of aerodynamic choking condition and its flow chart.

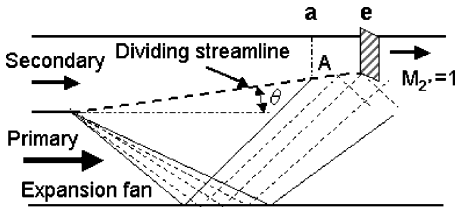

Fig. 4 Schematic diagram of model c for simulation of aerodynamic choking condition and its flow chart.

pointed out by Fabri and Siestrunck,[16] the pressure of the secondary flow is different from that of the primary flow in the one-dimensional isentropic model under conservation of mass, impulse function, and energy in a duct with a constant area.

Aerodynamic-Choking Model 2: Model C

Figure 4a shows a schematic of another aerodynamic-choking model. It is a further simplification of the model using the method of characteristics.[19] In this simplified model, the interaction between the primary flow and the secondary flow is calculated through impingement of a reflected expansion fan in the primary flow on the dividing streamline between the primary and secondary flows.

In this model, first, pressure of the secondary flow at the entrance is presumed. The primary flow expands to the pressure. Then, the dividing streamline between the primary flow and the secondary flow is drawn straight from the entrance to position a, where reflected expansion waves begin to impinge on the dividing streamline. The pressure in the secondary flow from the entrance to position a is simplified to be constant in this model. In the experiments, as shown in the section on experimental results, the pressure is approximately constant from the entrance of the test section to the beginning of the interaction between the expansion waves and the dividing streamline. The condition of the secondary flow at position a is calculated by subtraction of the reaction force from the secondary flow. The force is not transferred to the primary flow, and this is a contradiction in this simplified model.

The calculation of the primary flow with the method of characteristics is started from position a in the present simplified model. The angle of the dividing streamline downstream of position a is decided under the condition of pressure in the primary flow being equal to that in the secondary flow. In this model, the pressure of the secondary flow at the entrance is determined iteratively so that the secondary flow becomes sonic and parallel to the primary flow.

Results and Discussion

Wall Pressure Distribution

The wall pressure distributions with several parameters are presented to show an outline of the flow conditions. Positions of the aerodynamic choking, as well as amounts of entrained air, were calculated using the models. Results of these calculations are compared with the measured distributions of pressure.

Effects of the Total Pressure Ratio on the Pressure of the Mixture

Figure 5 shows the wall pressure distributions on the primary-flow side wall. The total pressure ratios, Pt_2/Pt_1, were 0.04 and 0.20. The area ratio of the secondary flow to the primary one was 0.81 with the height of 22 mm at the entrance. The solid symbols show the data under the throttling condition at the downstream throat. The open symbols show the data in the absence of throttling. Under that condition, there were pressure undulations caused by the reflection of shock waves and expansion waves and the levels of pressure were lower than those under the throttling condition. The wall pressure increased near the end of the test section due to the ambient pressure of the atmosphere.

Under the throttling condition at $Pt_2/Pt_1 = 0.04$, the wall pressure was the same as the pressure in the absence of throttling from the entrance to $x/H_1 = 11$. The high pressure in the downstream

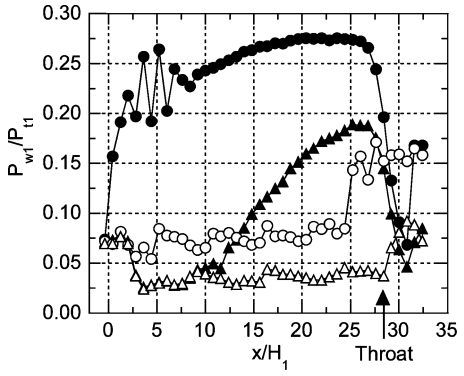

Fig. 5 Effect of ratio of total pressure on wall pressure distributions, $H_2 = 22$ mm and $M_1 = 2.4$: ●, $P_{t2}/P_{t1} = 0.20$, throttling; ▲, $P_{t2}/P_{t1} = 0.04$, throttling; ○, $P_{t2}/P_{t1} = 0.20$, no throttling; and △, $P_{t2}/P_{t1} = 0.04$, no throttling.

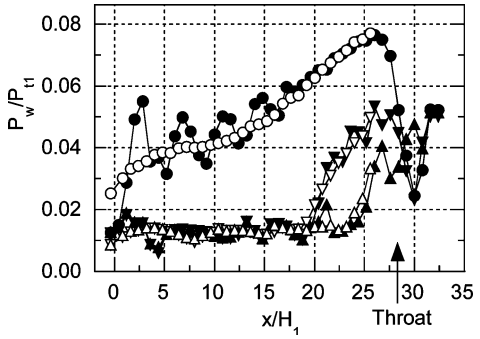

Fig. 6 Effect of Mach number on wall pressure distributions. $H_2 = 22$ mm and $M_1 = 3.4$: ●, $P_{t2}/P_{t1} = 0.04$, throttling, primary; ○, $P_{t2}/P_{t1} = 0.04$, throttling, secondary; ▼, $P_{t2}/P_{t1} = 0.02$, throttling, primary; ▽, $P_{t2}/P_{t1} = 0.02$, throttling, secondary; ▲, $P_{t2}/P_{t1} = 0.02$, no throttling, primary; and △, $P_{t2}/P_{t1} = 0.02$, no throttling, secondary.

region did not affect the pressure around the entrance of the test section. According to the measurement of the pitot pressure, the secondary flow was choked aerodynamically at around $x/H_1 = 6$. Under the throttling condition at $Pt_2/Pt_1 = 0.20$, shock waves and expansion waves were reflected on the primary-flow side wall only around the entrance of the test section. Downstream of $x/H_1 = 10$, the wall pressure increased and then decreased toward the downstream throat. The flow once decelerated to subsonic speed and then choked at the downstream throat. Under conditions of throttling, the larger the ratio of the total pressure of the secondary flow was, the higher the ratio of the maximum pressure to the total pressure of the primary flow in the test section.

Effect of the Mach Number of the Primary Flow

Figure 6 shows the wall pressure distributions on the primary- and the secondary-flow side walls at the Mach number of the primary flow of 3.4. The level of wall pressure at $M_1 = 3.4$ was one-third that at the $M_1 = 2.4$. Even under the $Pt_2/Pt_1 = 0.02$ condition of the underexpanded primary flow, choking at the downstream throat was difficult and the flow separated near $x/H_1 = 25$.

Model B and Model C Calculations

Figure 7 shows the pressure distributions calculated by model c. Measured pressures on the secondary-flow side wall for the no-throttling condition at $M_1 = 2.4$ and $H_2 = 30$ mm are also plotted for two different pressure ratios. Figure 8 shows a schlieren photograph around the entrance of the test section for the $P_{t2}/P_{t1} = 0.05$ condition. The distributions calculated by model c showed good agreement with the experimental results. The ends of the calculated line indicate the positions of the aerodynamic choking of the secondary flow. The choking positions of the secondary flow shown by pitot pressure measurement and the positions by model b are also indicated. The pitot pressure was measured at 5 mm from the secondary-flow side wall. The positions by model c showed good agreement with the measured ones. The positions by model b were located farther upstream than the measured ones. This was due to the simplicity of the model, which does not include the effect of reflection of the expansion fan.

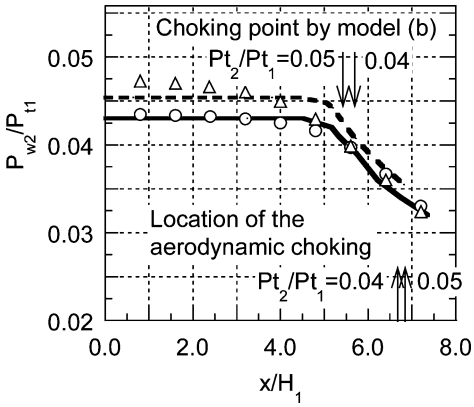

Fig. 7 Pressure distributions calculated by model c, choking positions of secondary flow calculated by model b, distributions measured on secondary-flow side wall, and choking points of secondary flow by pitot pressure measurement; $H_2 = 30$ mm and $M_1 = 2.4$: ○, $Pt_2/Pt_1 = 0.04$, $M_1 = 2.4$, $H_2 = 30$ mm; △, $Pt_2/Pt_1 = 0.05$, $M_1 = 2.4$, $H_2 = 30$ mm; ——, $Pt_2/Pt_1 = 0.04$, model c; and – – –, $Pt_2/Pt_1 = 0.05$, model c.

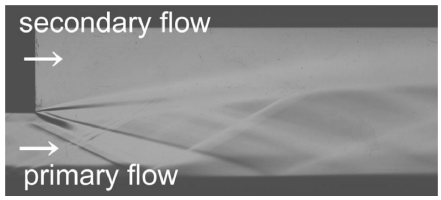

Fig. 8 Schlieren photograph around entrance of test section, $H_2 = 30$ mm, $M_1 = 2.4$, and $P_{t1}/P_{t1} = 0.05$.

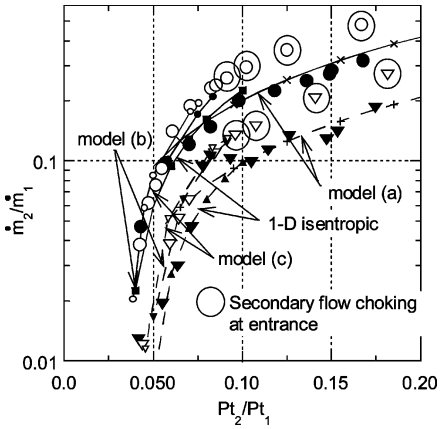

Fig. 9 Ratio of mass flow rate of secondary flow, $M_1 = 2.4$, and calculated mass flow rates of secondary fluid: ●, $H_2 = 30$ mm, throttling; ▼, $H_2 = 16$ mm, throttling; ○, $H_2 = 30$ mm, no throttling; ▽, $H_2 = 16$ mm, no throttling; ×, model a, $H_2 = 30$ mm; +, model a, $H_2 = 16$ mm; ●, model b, $H_2 = 30$ mm; ▾, model b, $H_2 = 16$ mm; ○, model c, $H_2 = 30$ mm; ▽, model c, $H_2 = 16$ mm; ■, one-dimensional isentropic, $H_2 = 30$ mm; and ▲, one-dimensional isentropic, $H_2 = 16$ mm.

Suction Performance

Effects of Total Pressure Ratio and Area Ratio

The results of the mass flow ratio are plotted against the total pressure ratio in Fig. 9. The solid and the open symbols show data under the throttling and no-throttling conditions, respectively. A large circle indicates the choking condition of the secondary flow

at the entrance. Under this condition, the mass flow ratio of the secondary flow was proportional to the ratio of the total pressures.

In the region where the total pressure ratio was larger than 0.05, the mass flow rate of the secondary flow decreased due to throttling at the downstream throat. Under this condition, the high downstream pressure affected the condition at the entrance of the test section so that the secondary flow was not choked. The ratio of the mass flow rate of the secondary flow increased with the increase of the ratio of the total pressure of the secondary flow. As the cross section of the secondary flow increased, the ratio of the secondary flow rate also increased. The results calculated with model a agreed well with the experimental results.

In the region of total pressure ratio smaller than about 0.05, the mass flow rate of the secondary flow did not choke at the entrance and was not affected by the downstream high pressure even under the throttling condition. In the absence of throttling, the mass flow rate of the secondary flow was not affected either. Under these conditions, the secondary flow choked aerodynamically and the downstream high pressure did not affect the flow conditions at the entrance. Figure 9 shows the secondary flow rates calculated by models b and c. The results of the two models agreed well with the experimental results. Under the aerodynamic choking condition, the suction performance of the secondary flow rate can be estimated with these models.

In Fig. 9, the results calculated with the one-dimensional isentropic procedure are also indicated as one-dimensional isentropic. In the calculation, properties of the primary and the secondary fluids were calculated under isentropic assumptions, for example, conservation of total pressure. The calculated amount of the entrained air agreed well with the experimental results at $H_2 = 30$ mm and was lower than the experimental results at $H_2 = 16$ mm. However, pressure of the secondary flow was about 30% higher than pressure of the primary flow at the aerodynamic choking point. Furthermore, this isentropic model cannot predict the length of interaction either.

Effect of the Mach Number of the Primary Flow

Figure 10 shows the effect of the primary flow Mach number on the mass flow rate of the secondary flow at $H_2 = 22$ mm. In the absence of throttling, there were no data for conditions with Pt_2/Pt_1 greater than 0.03 at $M_1 = 3.4$. Under this condition, the influence of the atmospheric pressure reached the entrance of the secondary flow duct.

The secondary flow choked aerodynamically below 0.015 of P_{t2}/P_{t1} under the Mach 3.4 condition of the primary flow. Under the Mach 2.4 condition of the primary flow, the secondary flow choked aerodynamically below 0.06 of P_{t2}/P_{t1} in the absence of throttling, and below 0.04 in the throttling condition. The results calculated with models b and c agreed with the experimental results under the aerodynamic choking condition. With the one-dimensional model employing the isentropic process throughout the interaction between the primary and the secondary flows, two pressures are calculated for each of the primary flow and the secondary flow.[16,17] Under the present experimental conditions, pressure of the secondary flow was about 50% higher than that of the primary flow under the Mach 3.4 condition at the aerodynamic choking point and about 20% higher under the Mach 2.4 condition.

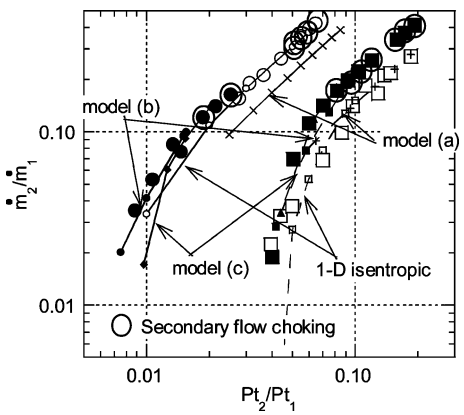

Fig. 10 Effect of Mach number of primary flow on secondary mass flow rate, $H_2 = 22$ mm: ●, $M_1 = 3.4$, no throttling; ■, $M_1 = 2.4$, no throttling; ○, $M_1 = 3.4$, throttling; □, $M_1 = 2.4$, throttling; ×, $M_1 = 3.4$, model a; +, $M_1 = 2.4$, model a; ●, $M_1 = 3.4$, model b; ■, $M_1 = 2.4$, model b; ◆, $M_1 = 3.4$, model c; ▲, $M_1 = 2.4$, model c; ○, $M_1 = 3.4$, one-dimensional isentropic; and □, $M_1 = 2.4$, one-dimensional isentropic.

The higher Mach number produced a greater secondary mass flow rate. This tendency resembled that shown by previous results.[16–18,24] The pressure at the entrance of the test section of the primary flow decreased with the increase of the Mach number. At the specified total pressure condition, the pressure at the entrance of the secondary flow then became small and the induced mass flow rate increased. In the lower level of the total pressure of the primary flow, however, Fabri and Siestrunck[16] and Fabri and Paulon[17] have reported that the mass flow rate of the secondary flow decreased with the increase of the Mach number of the primary flow. In the experiments by Fabri and Siestrunck, the cross section of the secondary flow at the entrance becomes smaller with an increase of the nozzle exit area of the primary flow and the flow rate of the secondary flow also becomes smaller. Under these conditions, the suction performance decreases with higher Mach number of the primary flow. On the other hand, in the present study, the nozzle throat area was smaller under the higher Mach number of the primary flow. The ratio of the mass flow rate of the secondary flow to that of the primary flow became larger at the same Pt_2/Pt_1 here.

Distributions of Mach Number and Mass Flux

Because the pressure of the inflow air is insufficient, sufficient mixing of the air with the rocket exhaust and deceleration of the mixture are required to attain high pressure in the diffuser section of the ejector-jet engine. Figures 11–14 show the distributions of the Mach number and the mass flux of the secondary fluid, respectively, on the center plane of the cross sections at $x/H_1 = 6.0$, 14.0, 22.0, and 25.2. The local mass flux of the secondary flow, $\rho_3 u_3 \omega$, is normalized with the mean mass flux of the secondary flow, $\dot{m}_2/A_3$. Under sufficient throttling conditions, the fluids were decelerated to subsonic speed and mixed as they passed through the pseudo-shock, whereas with no throttling or insufficient throttling, the primary and secondary fluids flowed out at supersonic speed and mixed due to the shear layer. Data showing the effect of ambient pressure at the exit are not plotted in Figs. 11–14.

Effect of Ratio of the Total Pressure

Figure 11 show the effect of the ratio of the total pressure on the Mach number and Fig. 12 show its effect on the mass flux distribution. Profiles in Figs. 11 and 13 were obtained by assuming constant static pressure across the flow, using the wall pressure. At $x/H_1 = 6$, the Mach numbers at $P_{t2}/P_{t1} = 0.08$ and 0.14 under the throttling condition were lower than those under the other conditions. Under these conditions, the downstream throttling affected the inflow conditions. At $x/H_1 = 25.2$, both the primary and the secondary flows were completely subsonic under the throttling condition. Even at $P_{t2}/P_{t1} = 0.04$, when the secondary flow choked aerodynamically and the downstream throttling did not affect the inflow condition of the secondary flow at the entrance, the flows mixed sufficiently due to the downstream throttling. Mass flux of the secondary flow showed a wide spread even at the beginning of the pseudo-shock, $x/H_1 = 14.0$ (Fig. 5). Fast and sufficient mixing was attained in the deceleration condition through the pseudo-shock. In the absence of throttling, even though the Mach number distribution was smooth in the supersonic region, the flows did not mix sufficiently.

Effects of the Area Ratio

Figure 13 show the effect of the area ratio on the Mach number and Fig. 14 show its effect on the mass flux distributions. The ratio of the total pressures of P_{t2}/P_{t1} was 0.04 and the Mach number of the primary flow was 2.4. Under these conditions, the throttling did not affect the condition of the secondary flow at the entrance. In

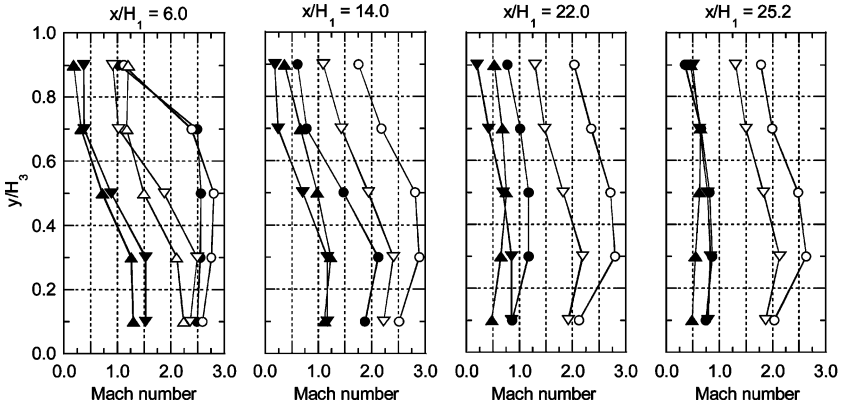

Fig. 11 Distributions of approximate Mach number, $H_2 = 22$ mm and $M_1 = 2.4$: ●, $P_{t2}/P_{t1} = 0.04$, throttling; ▼, $P_{t2}/P_{t1} = 0.08$, throttling; ▲, $P_{t2}/P_{t1} = 0.14$, throttling; ○, $P_{t2}/P_{t1} = 0.04$, no throttling; and ▽, $P_{t2}/P_{t1} = 0.08$, no throttling.

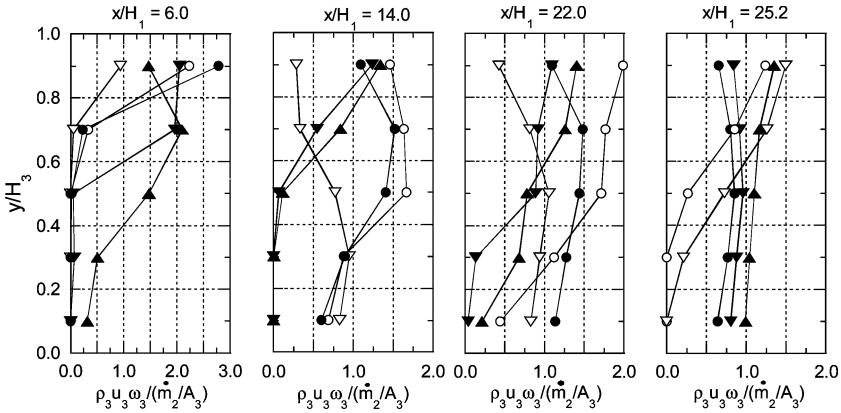

Fig. 12 Distributions of mass flux of the secondary flow, $H_2 = 22$ mm and $M_1 = 2.4$: ●, $P_{t2}/P_{t1} = 0.04$, throttling; ▼, $P_{t2}/P_{t1} = 0.08$, throttling; ▲, $P_{t2}/P_{t1} = 0.14$, throttling; ○, $P_{t2}/P_{t1} = 0.04$, no throttling; ▽, $P_{t2}/P_{t1} = 0.08$, no throttling; and △, $P_{t2}/P_{t1} = 0.14$, no throttling.

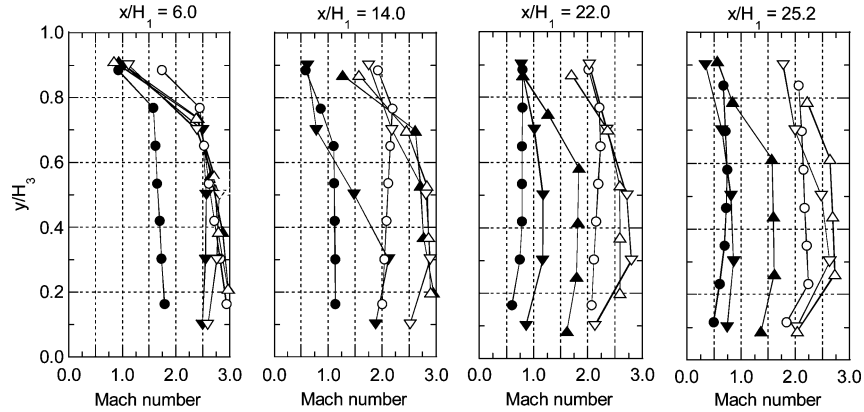

Fig. 13 Distributions of the approximate Mach number, $Pt_2/Pt_1 = 0.04$ and $M_1 = 2.4$: ●, $H_2 = 16$ mm, throttling; ▼, $H_2 = 22$ mm, throttling; ▲, $H_2 = 30$ mm, throttling; ○, $H_2 = 16$ mm, no throttling; ▽, $H_2 = 22$ mm, no throttling; and △, $H_2 = 30$ mm, no throttling.

the case of $H_2 = 30$ mm, however, the primary and secondary flows did not mix sufficiently and the primary flow remained supersonic and the secondary flow subsonic. Choking at the downstream throttled valve was not attained with a larger ratio of the height of the secondary flow to that of the primary flow. Under such condition, mixing was insufficient through the shear layer within a restricted length.

In the cases of $H_2 = 16$ and 22 mm under the throttling condition, the mixed flows were subsonic upstream of the downstream throat of $x/H_1 = 25.2$. The secondary flow under the $H_2 = 16$ mm condition choked aerodynamically, and the pseudo-shock was initiated from $x/H_1 = 3$ (not shown here). Though the mass flux of the secondary flow did not spread at $x/H_1 = 6$, it showed a wide spread at $x/H_1 = 14$. Again, fast and sufficient mixing was attained.

Total Pressure Increase

An increase of pressure in the diffuser section due to sufficient mixing is necessary for thrust augmentation of the ejector-jet. The ratios of total pressure of the mixture to that of the primary flow, P_{t3}/P_{t1}, under the throttling condition are in Fig. 15. P_{t3} was calculated with the average Mach number and the wall pressure at $x/H_1 = 25.2$. The higher the ratio of the total pressures and the smaller the height of the secondary flow entrance, the larger is the ratio of the mass flow rate of the primary flow and the larger is the

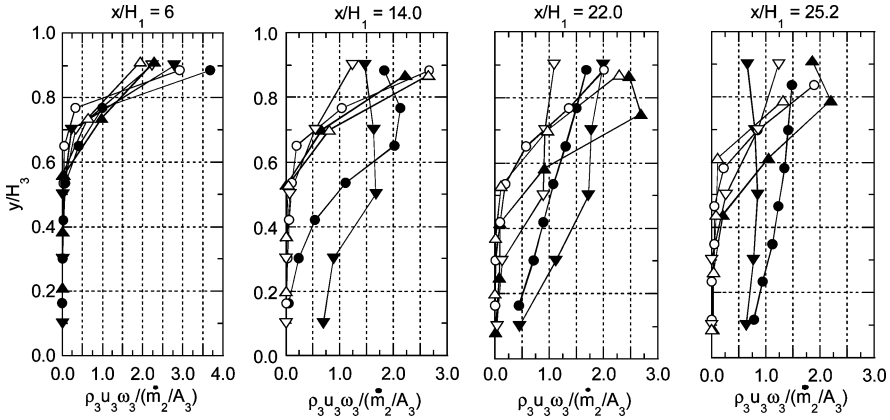

Fig. 14 Distributions of the mass flux of the secondary flow, $Pt_2/Pt_1 = 0.04$ and $M_1 = 2.4$: ●, $H_2 = 16$ mm, throttling; ▼, $H_2 = 22$ mm, throttling; ▲, $H_2 = 30$ mm, throttling; ○, $H_2 = 16$ mm, no throttling; ▽, $H_2 = 22$ mm, no throttling; and △, $H_2 = 30$ mm, no throttling.

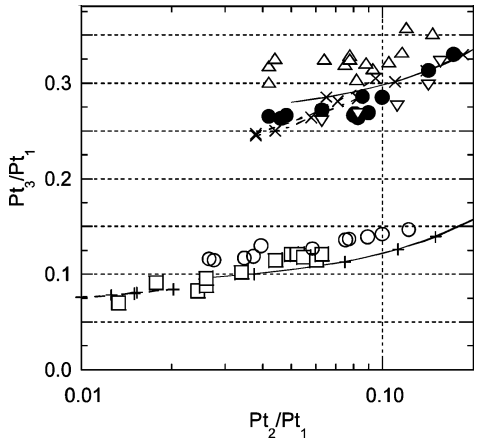

Fig. 15 Effect of ratio of total pressures, Pt_2/Pt_1, on total pressure of the mixture and calculated total pressures of mixture: △, $M_1 = 2.4$, $H_2 = 16$ mm; ●, $M_1 = 2.4$, $H_2 = 22$ mm; ▽, $M_1 = 2.4$, $H_2 = 30$ mm; □, $M_1 = 3.4$, $H_2 = 22$ mm; ○, $M_1 = 3.4$, $H_2 = 16$ mm; —×—, model a, $M_1 = 2.4$, $H_2 = 22$ mm; - - × - -, Downstream choking and model b, $M_1 = 2.4$, $H_2 = 22$ mm; · · · × · · ·, Downstream choking and model c, $M_1 = 2.4$, $H_2 = 22$ mm; – – + – –, model a, $M_1 = 3.4$, $H_2 = 22$ mm; - - + - - , Downstream choking and model b, $M_1 = 3.4$, $H_2 = 22$ mm; and · – + – ·, Downstream choking and model c, $M_1 = 3.4$, $H_2 = 22$ mm.

total pressure of the mixture. The total pressure level of the $M_1 = 3.4$ condition was about one-third that of the $M_1 = 2.4$ condition. The results by model a agreed well with the experimental results.

To predict the total pressure of the mixture, P_{t3}, in the aerodynamic choking condition, the downstream choking condition was combined with model b or model c for the suction condition. The mass flow rate of the secondary flow was calculated with model b or model c. The calculated flow rate was used as a boundary condition, in addition to P_{t1} and $\dot{m}_1$. With these boundary conditions and the choking condition at the downstream throat, the total pressure of the mixture was calculated. The total pressure of the secondary flow was also calculated, but such a calculated value is not usually equal to the total pressure of the secondary flow applied in the experiments and used to calculate the mass flow rate of the secondary flow. This is a contradiction from the combination of models in relation to the actual flow conditions. The model was applied to the test condition from the engineering viewpoint here. Figure 15 shows that the pressures calculated with the model under the condition of $H_2 = 22$ mm approximately agreed with the experimental values. The calculated results under the condition $H_2 = 16$ mm also agreed with the experimental results, which are not plotted in Fig. 15. In the present experimental conditions, the combination model approximately predicted the total pressure of the mixture.

The pressure recovery of the mixture is discussed here. Mass flow rate of the mixture is expressed as follows under the choking condition at the downstream throat:

$$\dot{m}_3 = A_{\text{th}} \cdot P_{t3}\sqrt{\gamma/R \cdot T_t}\left\{1/[(\gamma+1)/2]^{(\gamma+1)/2(\gamma-1)}\right\} \quad (1)$$
$$= \dot{m}_1 + \dot{m}_2$$
$$= (1+r) \cdot \dot{m}_1$$

Isentropic change in the convergent section is presumed. Here,

$$r = \dot{m}_2/\dot{m}_1 \quad (2)$$

Mass flow rate of the primary flow is as follows:

$$\dot{m}_1 = A_1 \cdot P_{t1}\sqrt{\gamma/R \cdot T_t} \cdot M_1 \cdot \left(1\Big/\left\{1+[(\gamma-1)/2]M_1^2\right\}^{(\gamma+1)/2(\gamma-1)}\right) \quad (3)$$

With Eqs. (1) and (3), the following relation is derived:

$$\frac{P_{t3}}{P_{t1}} = \frac{A_1(1+r)}{A_{\text{th}}} \cdot M_1 \cdot \left\{\frac{(\gamma+1)/2}{1+[(\gamma-1)/2]M_1^2}\right\}^{(\gamma+1)/2(\gamma-1)} \quad (4)$$

Around $r = 0$–0.5 and under the fixed contraction ratio of A_1/A_{th}, total pressure of the mixture, P_{t3}, becomes smaller at larger Mach number of the primary flow, M_1, in the supersonic ejector. The decreasing factor depends on the Mach number, as shown in Eq. (4). As the Mach number of the primary flow decreases to unity, the total pressure of the mixture, Pt_3, becomes large and the total pressure loss becomes small. When the total pressure of the secondary flow increases, the mass flow rate increases and the total pressure of the mixture increases. As shown in the preceding section, however, the suction performance decreases with the decrease of the Mach number of the primary flow.

In some studies,[18,24] the pressure of the mixture has been found to be larger at higher Mach number of the primary flow. However, this opposite finding resulted from different specifications of the test conditions or different ways of indicating the test results than those of the present study. In one such study,[18] the throat section of the primary flow was specified. Thus, the mass flow rate of the primary flow was proportional to the total pressure of the primary flow. As shown in an earlier section, the mass flow rate of the secondary fluid increased with the increase of the Mach number of the primary flow due to the increase of the suction performance. Under such a condition, Pt_3 increases with the increase of the Mach number of the primary flow. In another study,[24] the total pressure of the mixture was normalized by the total pressure of the secondary flow. When the total pressure of the primary flow was used for normalization, the total pressure of the mixture increased with the decrease of the Mach number of the primary flow.

Conclusions

Aerodynamic tests of the ejector-jet were conducted. Evaluation of a new one-dimensional model of suction performance under the aerodynamic-choking condition and observation of the mixing process through the pseudo-shock were primary subjects of the present study. The parameters were the ratio of the total pressures, the ratio of the entrance areas, and the Mach number of the primary flow. The investigation clarified the following points.

1) The suction performance could be predicted well with the new one-dimensional model, in which pressures of the primary and the secondary flows were the same.

2) The position of the aerodynamic choking predicted with the new one-dimensional model was upstream of the measured one, as shown by the lack of effect of reflection of the expansion waves of the primary flow. The position could be predicted well with a model using the method of characteristics.

3) Sufficient mixing was attained in the deceleration process to subsonic speed through the pseudo-shock. Mixing progressed quickly in the pseudo-shock.

Acknowledgments

The authors are grateful to Shinji Kubota, a graduate student of Tohoku University, for his help in conducting the experiment.

References

[1]Escher, W., "A U.S. History of Airbreathing/Rocket Combined-Cycle(RBCC) Propulsion for Powering Future Aerospace Transports, with a Look Ahead to the Year 2020," International Society for Air Breathing Engines, Paper ISABE 99-7028, Sept. 1999.

[2]Heiser, W. H., Pratt, D. T., Daley, D. H., and Mehta, U. B., "Hypersonic Airbreathing Propulsion," AIAA Education Series, AIAA, Reston, VA, 1994, pp. 446–451, 456–472.

[3]Foster, R. W., Escher, W. J. D., and Robinson, J. W., "Studies of an Extensively Axisymmetric Rocket Based Combined Cycle (RBCC) Engine Powered SSTO Vehicle," AIAA Paper 89-2294, July 1989.

[4]Daines, R., and Segal, C., "Combined Rocket and Airbreathing Propulsion Systems for Space-Launch Applications," *Journal of Propulsion and Power*, Vol. 14, No. 5, 1998, pp. 605–611.

[5]Olds, J. R., and Bradford, J. E., "SCCREAM: A Conceptual Rocket-Based Combined-Cycle Engine Performance Analysis Tool," *Journal of Propulsion and Power*, Vol. 17, No. 2, 2001, pp. 333–339.

[6]Thomas, S. R., Palac, D. T., Trefny, C. J., and Roche, J. M., "Performance Evaluation of the NASA GTX RBCC Flowpath," International Society for Air Breathing Engines, Paper ISABE 2001-1070, Sept. 2001.

[7]Campbell, B. T., Siebenhaar, A., and Nguyen, T., "Strutjet Engine Performance," *Journal of Propulsion and Power*, Vol. 17, No. 6, 2001, pp. 1227–1232.

[8]Kanda, T., and Kudo, K., "Conceptual Study of a Combined-Cycle Engine for an Aerospace Plane," *Journal of Propulsion and Power*, Vol. 19, No. 5, 2003, pp. 859–867.

[9]Peters, C. E., Phares, W. J., and Cunningham, T. H. M., "Theoretical and Experimental Studies of Ducted Mixing and Burning of Coaxial Streams," *Journal of Spacecraft and Rockets*, Vol. 6, No. 12, 1969, pp. 1435–1441.

[10]Masuya, G., Chinzei, N., and Ishii, S., "A Study on Air Breathing Rockets—Subsonic Mode Combustion," *Acta Astronautica*, Vol. 8, No. 5-6, 1981, pp. 643–661.

[11]Chinzei, N., Masuya, G., Kudou, K., Murakami, A., and Komuro, T., "Experiment on Multiple Fuel Supplies to Airbreathing Rocket Combustors," *Journal of Propulsion and Power*, Vol. 3, No. 1, 1987, pp. 26–32.

[12]Daines, R. L., and Merkle, C. L., "Computational Fluid Dynamic Modeling of Rocket Based Combined Cycle Engine Flowfields," AIAA Paper 94-3327, June 1994.

[13]Dijkstra, F., Maree, A. G. M., Caporicci, M., and Immich, H., "Experimental Investigation of the Thrust Enhancement Potential of Ejector Rockets," AIAA Paper 97-2756, July 1997.

[14]Lehman, M., Pal, S., and Santoro, R. J., "Experimental Investigation of the RBCC Rocket-Ejector Mode," AIAA Paper 2000-3725, July 2000.

[15]Han, S., Peddieson, J., Jr., and Gregory, D., "Ejector Primary Flow Molecular Weight Effects in an Ejector-Ram Rocket Engine," *Journal of Propulsion and Power*, Vol. 18, No. 3, 2002, pp. 592–599.

[16]Fabri, J., and Siestrunck, R., "Supersonic Air Ejectors," *Advances in Applied Mechanics*, Vol. 5, Academic Press, New York, 1958, pp. 1–34.

[17]Fabri, J., and Paulon, J., "Theory and Experiments on Supersonic Air-to-Air Ejectors," NACA TM 1410, Jan. 1958.

[18]Dello, R. V., Rose, R. E., and Dart, R. S., "An Experimental Investigation of the Use of Supersonic Driving Jets for Ejector Pumps," *Journal of Engineering for Power*, April 1962, pp. 204–212.

[19]Chow, W. L., and Addy, A. L., "Interaction Between Primary and Secondary Streams of Supersonic Ejector Systems and Their Performance Characteristics," *AIAA Journal*, Vol. 2, No. 4, 1964, pp. 686–695.

[20]Emanuel, G., "Optimum Performance for a Single-Stage Gaseous Ejector," *AIAA Journal*, Vol., 14, No. 9, 1976, pp. 1292–1296.

[21]Dutton, J. C., Mikkelsen, C. D., and Addy, A. L., "A Theoretical and Experimental Investigation of the Constant Area, Supersonic-Supersonic Ejector," *AIAA Journal*, Vol. 20, No. 10, 1982, pp. 1392–1400.

[22]Alperin, M., and Wu, J.-J., "Thrust Augmenting Ejectors, Part 1," *AIAA Journal*, Vol. 21, No. 10, 1983, pp. 1428–1436.

[23]Dutton, J. C., and Carroll, B. F., "Optimal Supersonic Ejector Designs," *Journal of Fluids Engineering*, Vol. 108, No. 4, 1986, pp. 414–420.

[24]Petersen, E. L., Roan, V. P., and Pfahler. J. N., "Experimental Investigation of Supersonic-Primary Dissimilar-Fluid Ejectors," AIAA Paper 92-3793, July 1992.

[25]Matsuo, K., Miyazato, Y., and Kim, H.-D., "Shock Train and Pseudo-Shock Phenomena in Internal Gas Flows," *Progress in Aerospace Sciences*, Vol. 35, No. 2, 1999, pp. 33–100.

[26]Carroll, B. F., and Dutton, J. C., "Turbulence Phenomena in a Multiple Normal Shock Wave/Turbulent Boundary-Layer Interaction," *AIAA Journal*, Vol. 30, No. 1, 1992, pp. 43–48.

[27]Ogawa, S., Choi, B., Takita, K., and Masuya, G., "Fuel Mixing Enhancement by Pre-Combustion Shock Wave," International Society for Air Breathing Engines, Paper ISABE 2001-1188, Sept. 2001.

[28]Seiner, J. M., Dash, S. M., and Kenzakowski, D. C., "Historical Survey on Enhanced Mixing in Scramjet Engines," *Journal of Propulsion and Power*, Vol. 17, No. 6, 2001, pp. 1273–1286.